Catalysis Science & Technology

ROYAL SOCIETY OF CHEMISTRY

PAPER

View Article Online
View Journal | View Issue

Cite this: *Catal. Sci. Technol.*, 2023, **13**, 6839

Structure-based insights into mechanism of endoperoxidase FtmOx1 catalyzed reactions†

Fei Wang,[ad] Yanqing Gao,[b] Chunxi Wang,[a] Wenxian Lan,[c] JianHua Gan*[b] and Chunyang Cao *[ad]

Received 18th January 2023,
Accepted 20th February 2023

DOI: 10.1039/d3cy00092c

rsc.li/catalysis

FtmOx1 is an α-ketoglutarate (α-KG) dependent mononuclear non-haem iron enzyme, which catalyzes endoperoxidation in fumitremorgin B to form verruculogen. The main products of the reaction are extremely complicated depending on the different conditions. Two mechanisms, COX-like and CarC-like, were reported, mainly debating which residue Y224 or Y68 is a key determinant in ftmOx1 catalytic endoperoxidation. To address this, here, we performed structural analysis of three binary complexes, ftmOx1·Fe^{2+}·α-KG (4Y5S), ftmOx1 Y68F·Co^{2+}·α-KG (7ETL) and ftmOx1 Y140F·Fe^{2+}·α-KG (6OXH), and of two ternary complexes, ftmOx1·Co^{2+}·α-KG·13-oxo fumitremorgin B (7WSB) and ftmOx1·Fe^{2+}·α-KG·fumitremorgin B (7ETK). We found that residue Y224 forms a hydrogen bond with α-KG, which implies that Y224 potentially suppresses oxygen rebound reaction by forming a hydrogen bond with oxo-ferry species and enhances the endoperoxidation selectivity of wild-type ftmOx1. Substrate insertion into the Fe^{2+} binding pocket results in the generation of a new conformation of Y224, in line with the observed structures of 7ETK and 7WSB. This conformation of Y224 is fixed by forming a hydrogen bond with the residue T134 –OH group. The mutations of residue T134 led to major products of oxygen rebound and dealkylation, suggesting that it acts as a regulator of the reactions. Possible reaction pathways were suggested, demonstrating how Y68, T134 and Y224 work together in ftmOx1 catalyzed reactions.

Introduction

Endoperoxides possess diverse bioactivity, including antimalarial, antitumor, and antimicrobial activities, and so on.[1,2] However, there are many challenges to obtaining endoperoxides in high yields and of pure quality through total organic synthesis. FtmOx1, a novel non-haem iron enzyme, was reported to catalyze O_2 installation between the C-21 and C-27 atoms of fumitremorgin B (compound **1**) without O–O bond scission (major products 2 and 3, Scheme 1).[2–6] However, the outcomes of the ftmOx1-involved reactions are too complicated based on the different conditions. In the absence of ascorbate, using compound **1** as the substrate, the main products of the wild-type ftmOx1 catalyzed reaction are compound **3** (Scheme 1a),[4] while the main products of the ftmOx1 Y224F variant catalyzed reaction are the oxygen rebound and dealkylation product compounds **4** and **5** (Scheme 1b).[4] In contrast, using the same substrate, in the presence of excess ascorbate, the main product of wild-type ftmOx1 and its Y74F, Y140F and even Y224F variant catalyzed reaction is compound **2** (Scheme 1c),[2] while the main product of the ftmOx1 Y68F catalyzed reaction is compound **6** (Scheme 1d).[2,5] Using 13-oxo fumitremorgin B (compound **7**) as the substrate, the major product is dealkylation compound **5** (Scheme 1e).[4] Furthermore, the wild-type ftmOx1 can even catalyze the direct transformation from compound **2** to **3** (Scheme 1f) in the absence or in the presence of ascorbate.[4] In an excess of Fe^{2+} and ascorbate, ftmOx1 oxidizes compound **2** into compound **8** (Scheme 1f).[4] The structure of ftmOx1 in complex with its co-factor α-ketoglutarate (α-KG) (*i.e.*, the binary complex ftmOx1·Fe^{2+}·α-KG, pdb code 4Y5S) shows that ftmOx1 might act in a cyclooxygenase (COX)-like mechanism (Fig. S1a†), identical to other endoperoxide-installing enzymes such as COX-1 and COX-2.[7] In the COX-like mechanism, the residue Y224 donates hydrogen to the Fe(IV)=O species (forming Y224-O$^{\bullet}$), and Y224-O$^{\bullet}$ performs a hydrogen-abstraction transfer (HAT) from the C-21 atom of fumitremorgin B.[4] This mechanism was supported by the fact

[a] *State Key Laboratory of Bioorganic and Natural Product Chemistry, Center for Excellence in Molecular Synthesis, Shanghai Institute of Organic Chemistry, Chinese Academy of Sciences, 345 Lingling Road, Shanghai, 200032, China. E-mail: ccao@mail.sioc.ac.cn; Tel: +86 21 54925491*
[b] *Department of Physiology and Biophysics, School of Life Sciences, Fudan University, Shanghai 200433, China. E-mail: ganjhh@fudan.edu.cn*
[c] *The Core Facility Centre of CAS Center for Excellence in Molecular Plant Sciences, 300 Fengling Road, Shanghai, 200032, China*
[d] *University of Chinese Academy of Science, No. 19A, Yuquan Road, Shijingshan District, Beijing, 100049, China*

† Electronic supplementary information (ESI) available. See DOI: https://doi.org/10.1039/d3cy00092c

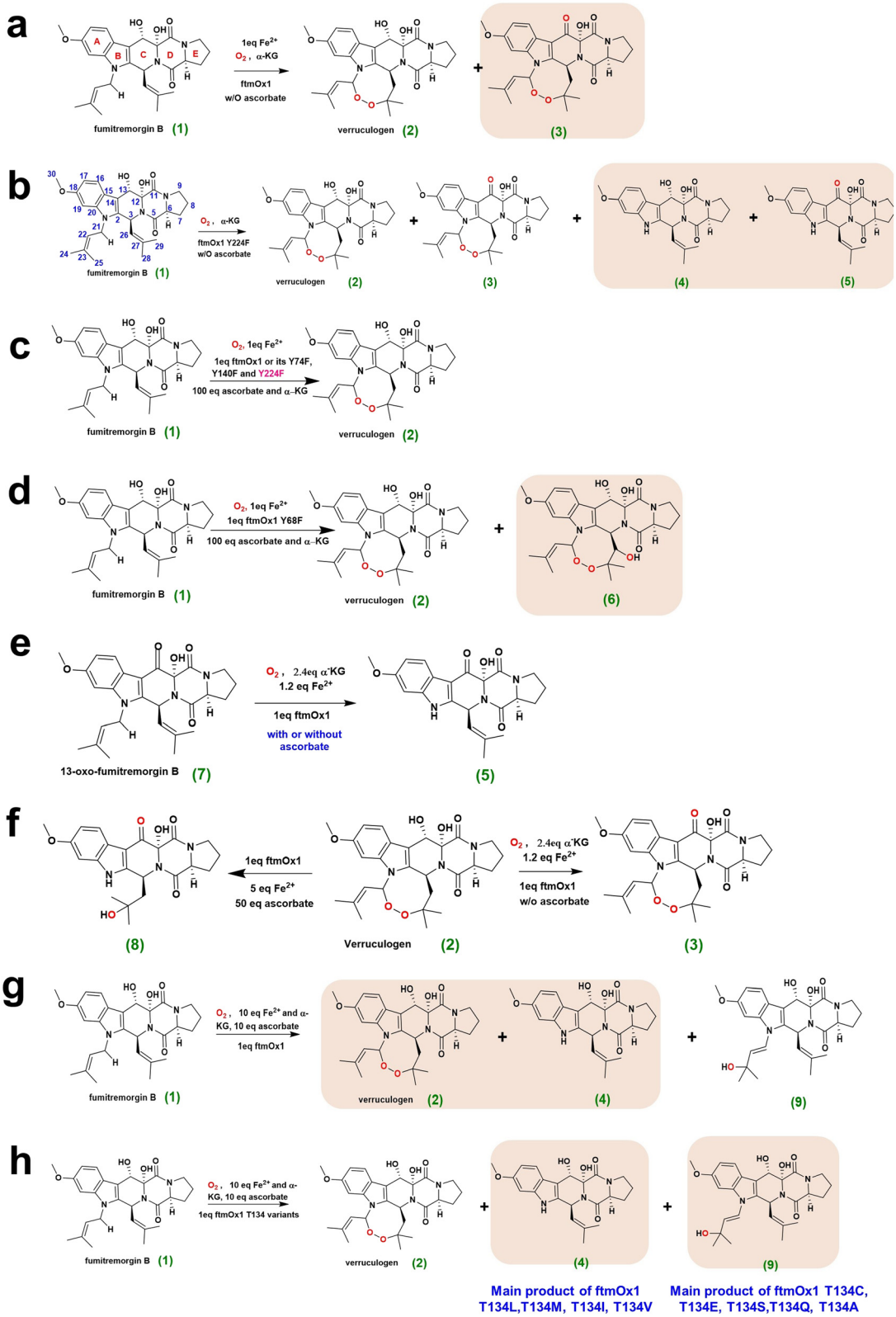

Scheme 1 FtmOx1 or its variant catalysed reactions using fumitremorgin B (compound **1**), its 13-oxo analogue (compound **7**) and verruculogen (compound **2**) as the substrates. (a–f) Reported ftmOx1-catalysis outcomes under different conditions observed for the wild-type ftmOx1 enzyme and its variants; (g and h) FtmOx1 and its T134 variant catalysed reactions in this manuscript. In (a and b), the rings A, B, C, D and E and the numbers of all carbon atoms of the substrate fumitremorgin B (**1**) are labelled for clear description of the reactions in the manuscript. The main products of the reactions are all in orange boxes.

that hydrogen transfer from Y224 to Fe(IV)=O only needs to overcome a very low energy barrier of 6.4 kcal mol^{-1}.[8]

However, based on the results from stop flow assay and EPR assay, Dunham *et al.*, suggested a CarC-like mechanism (Fig. S1b†), in which the first tyrosine radical is formed at residue Y68.[2] The Fe(IV)=O species directly abstracts hydrogen from the C-21 atom of fumitremorgin B, then O_2 is installed between the C-21 and C-27 atoms of fumitremorgin B. The radical is transported to the C-26 atom (C26$^{\bullet}$). Next, the radical C26$^{\bullet}$ abstracts hydrogen from the hydroxyl group of residue Y68 (forming radical Y68-O$^{\bullet}$). Finally, the reductant ascorbic acid reduces Fe(III)–OH into Fe(II) and the Y68 radical Y68-O$^{\bullet}$ into Y68 for the next catalytic cycle.[2,5] This mechanism was further confirmed by using noncanonical halogenated tyrosine or amino phenylalanine analogues in place of Y68 and Y224.[5] The crystal structure of ftmOx1 in complex with Fe^{2+}, α-KG and fumitremorgin B (*i.e.*, the ternary complex ftmOx1·Fe^{2+}·α-KG·fumitremorgin B, pdb code 7ETK)[6] confirmed that fumitremorgin B binding induces significant compression of the iron ion binding active pocket; Y68 is close to the C-26 atom of the substrate fumitremorgin B through hydrophobic interactions with the rings B and C of the substrate (Scheme 1a), thus supporting the CarC-like mechanism. However, the CarC-like mechanism cannot interpret the roles of the residue Y224 in ftmOx1 catalyzed reactions.

Results and discussion

Indications from ^{19}F-NMR experiments

To ascertain the mechanism of ftmOx1-involved catalytic reactions, we firstly decided to test which residue, Y224 or Y68, is involved in the substrate binding using ^{19}F-NMR experiments. It is well known that the ^{19}F nucleus has 100% natural abundance with 1/2 nuclear spin, presenting highly sensitive and steady NMR signals along with its surrounding chemical environment because of the unpaired electron in the outer shell of the ^{19}F atom.[9–11] Different ^{19}F-labeled amino acids, for example, 3-flourine-L-tyrosine, have been reported to be introduced into proteins without any influences on the protein's local or global folding or their biological functions.[10] Thus, ^{19}F-labeled amino acids were used to detect possible conformation changes in hydrophobicity and solvent exposed surface area upon substrate binding.[9]

There are six tyrosines (*i.e.*, Y68, Y74, Y102, Y109, Y224 and Y239) in total in wild-type ftmOx1. In structures of ftmOx1·Fe^{2+} (pdb code 4Y5T) and the binary complex ftmOx1·Fe^{2+}·α-KG (4Y5S), residues Y68 and Y224 are much closer to the catalytic Fe^{2+} binding centre than the other tyrosines. The distance between the iron ion and Y68-O atom is 11.9 Å, while the distance between the iron ion and Y224-O atom is only 4.2 Å. The differences in the reported COX-like and CarC-like mechanisms mainly lie in the roles of the residues Y68 and Y224 in ftmOx1 catalytic reactions. Therefore, to ensure that the ^{19}F-NMR signal is generated from a single 3-flourine-L-tyrosine in ftmOx1, we mutated all tyrosines (Tyr) except Y68 and Y224 into phenylalanines (Phe). Two NMR samples, only the ^{19}F-labeled Y68 containing ftmOx1 variant (*i.e.*, the ^{19}F-Y68 labelled ftmOx1 Y74/102/109/224/239F variant) and only the ^{19}F-labeled Y224 containing ftmOx1 variant (*i.e.*, the ^{19}F-Y224 ftmOx1 Y68/74/102/109/239F variant), were firstly prepared.

In addition, in the structure of 4Y5S, the residue L222 locates *trans* to residue Y68 (Fig. 1a). To test which side (L222 or Y68) of the iron ion binding centre could be the substrate binding site in solution, we made another NMR sample, the ftmOx1 L222Y variant containing only ^{19}F-labelled Y222 (*i.e.*, ^{19}F-Y222 ftmOx1, Y68/74/102/109/224/239F and L222Y). During NMR data acquisition, we could not keep our NMR samples in an anaerobic environment. At the same time, the structure of the ftmOx1·Fe^{2+} complex (4Y5T) can be superimposed well over the structure of the ftmOx1·Fe^{2+}·α-KG binary complex (4Y5S) (RMSD = 0.14 Å), revealing that α-KG ligating to Fe^{2+} does not result in significant conformational changes of ftmOx1. The local conformations of residues Y68 and Y224 slightly rotate by an angle smaller than 10° (Fig. S2†). Thus, to avoid catalytic reaction and to obtain a stable complex, we just mixed each ^{19}F-labelled ftmOx1 variant with the substrate fumitremorgin B at a molar ratio of 1 : 1 (ftmOx1 *vs.* substrate) in the absence of α-KG and ascorbate. Then, we performed ^{19}F-NMR experiments on the free ^{19}F-labelled ftmOx1 variants and their complexes with the substrate (Fig. 1b–d). Obviously, before adding the substrate, there is more than one signal belonging to free ^{19}F-Y222 and ^{19}F-Y224, suggesting that residues Y222 and Y224 are flexible; at least two conformations of them are in the iron ion binding centre. After adding the substrate, a new ^{19}F-NMR signal appeared in the downfield region of the spectrum acquired on the sample of the ftmOx1 variant containing only ^{19}F-Y224 mixed with the substrate (Fig. 1b). At the same time, the ^{19}F-NMR signals belonging to free ^{19}F-Y224 remained unchanged, implying that substrate binding results in the generation of a new conformation of residue Y224, and there is an equilibrium between the free and bound states of residue Y224 in solution, which is consistent with the reported structure of ftmOx1·Co^{2+}·α-KG·13-oxo fumitremorgin B ternary complex (7WSB).[4] In structure 7WSB,[4] the substrate analogue 13-oxo fumitremorgin B was used to probe the mechanism of endoperoxidation of the substrate. At the same time, Fe^{2+} was replaced with Co^{2+}, which generated a stable complex involved in the beginning of ftmOx1 catalytic reaction. In this structure, residue Y224 has two conformations. As shown in Fig. 2a, when the three crystal structures 4Y5S, 7WSB and 7ETK are superimposed, the backbone atoms of the proteins overlap well with an RMSD value of 0.78 Å. The position of the substrate fumitremorgin B in structure 7ETK is almost identical to that of 13-oxo fumitremorgin B in structure 7WSB. In structure 7WSB, one conformation of Y224 is similar to that in structure 7ETK, and the other is almost identical to that in structure 4Y5S. Therefore, interaction between the substrate

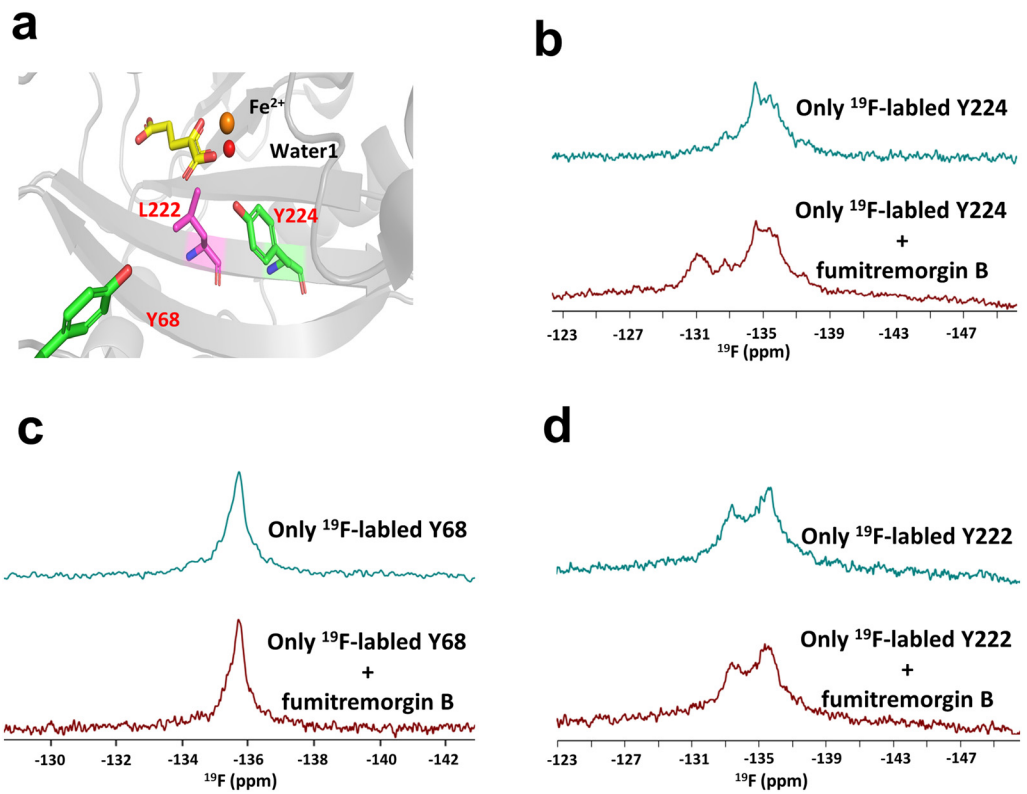

Fig. 1 The new conformation of the residue Y224 is generated due to substrate binding, and detected by one-dimensional ^{19}F-NMR titration experiments. (a) The positions of residues Y68, L222 and Y224 relative to α-KG and the iron ion in the structure of the ftmOx1·Fe^{2+}·α-KG binary complex (4Y5S). The orange ball represents the iron ion. The red ball represents water 1. The protein was drawn in grey transparent cartoon mode. The residues Y68, L222 and Y224 were drawn in green or pink stick mode. (b) ^{19}F-NMR titration performed on the ftmOx1 variant containing only ^{19}F-Y224 and its mixture with fumitremorgin B. (c) ^{19}F-NMR titration performed on the ftmOx1 variant containing only ^{19}F-Y68 and its mixture with fumitremorgin B. (d) ^{19}F-NMR titration performed on the ftmOx1 variant containing only ^{19}F-Y222 and its mixture with fumitremorgin B. The molar ratio of enzyme to substrate is 1 : 1.

and the enzyme results in the generation of a new conformation of the residue Y224.

In contrast, no significant signal changes were observed and no new signals appeared in the spectra acquired on either the ftmOx1 variant containing only ^{19}F-Y68 or the ftmOx1 variant containing only ^{19}F-Y222 mixed with the substrate (Fig. 1c and d), indicating that substrate binding does not lead to a large perturbation of the conformation of the residues Y68 and Y222. However, different from structure 4Y5S, the side-chain aromatic ring of residue Y68 in structures 7ETK and 7WSB locates over the rings B and C (Fig. 2a) of fumitremorgin B or its analogue 13-oxo fumitremorgin B through hydrophobic interactions. With reference to the position of Y68 in structure 4Y5S, the –OH group of Y68 moves 4.5 Å in structure 7WSB and 5.0 Å in structure 7ETK, respectively. We were confused as to why no new ^{19}F-NMR signal and/or chemical shift change of the ^{19}F-NMR signal was observed when the ^{19}F-labelled Y68 ftmOx1 variant was mixed with the substrate.

To account for this, we decided to analyze the reported structures. In contrast to the location of residue Y224 in one rigid β-sheet of ftmOx1, Y68 locates on the flexible region (55-72 aa) of ftmOx1, which contains one α-helix (64-68 aa). In structure 4Y5S, Y68 is solvent accessible. The substrate fumitremorgin B and its analogue 13-oxo fumitremorgin B are hydrophobic. Their insertion into the iron ion binding pocket enables Y68 to move easily due to hydrophobic interactions between them, which results in compression of the iron ion binding pocket. In structures 7ETK and 7WSB, Y68 is still exposed to the solvent. The conformational compression of the iron ion binding pocket does not obviously change the solvent exposed area of Y68, which might make it impossible for ^{19}F-NMR to detect conformational changes of Y68. In addition, Y68 is almost parallel to the aromatic rings A and B of fumitremorgin B and its analogue 13-oxo fumitremorgin B, and the anisotropy effect of these two aromatic rings could also balance the theoretical chemical shift changes of the ^{19}F-NMR signal of bound ^{19}F-Y68 resulting from its local conformational changes.

Roles of residue Y224 in ftmOx1 catalyzed reactions

To probe how Y224 works in the ftmOx1 catalytic reactions, we tried to obtain the crystal structure of the ftmOx1 Y224F variant in complex with the substrate fumitremorgin B. To

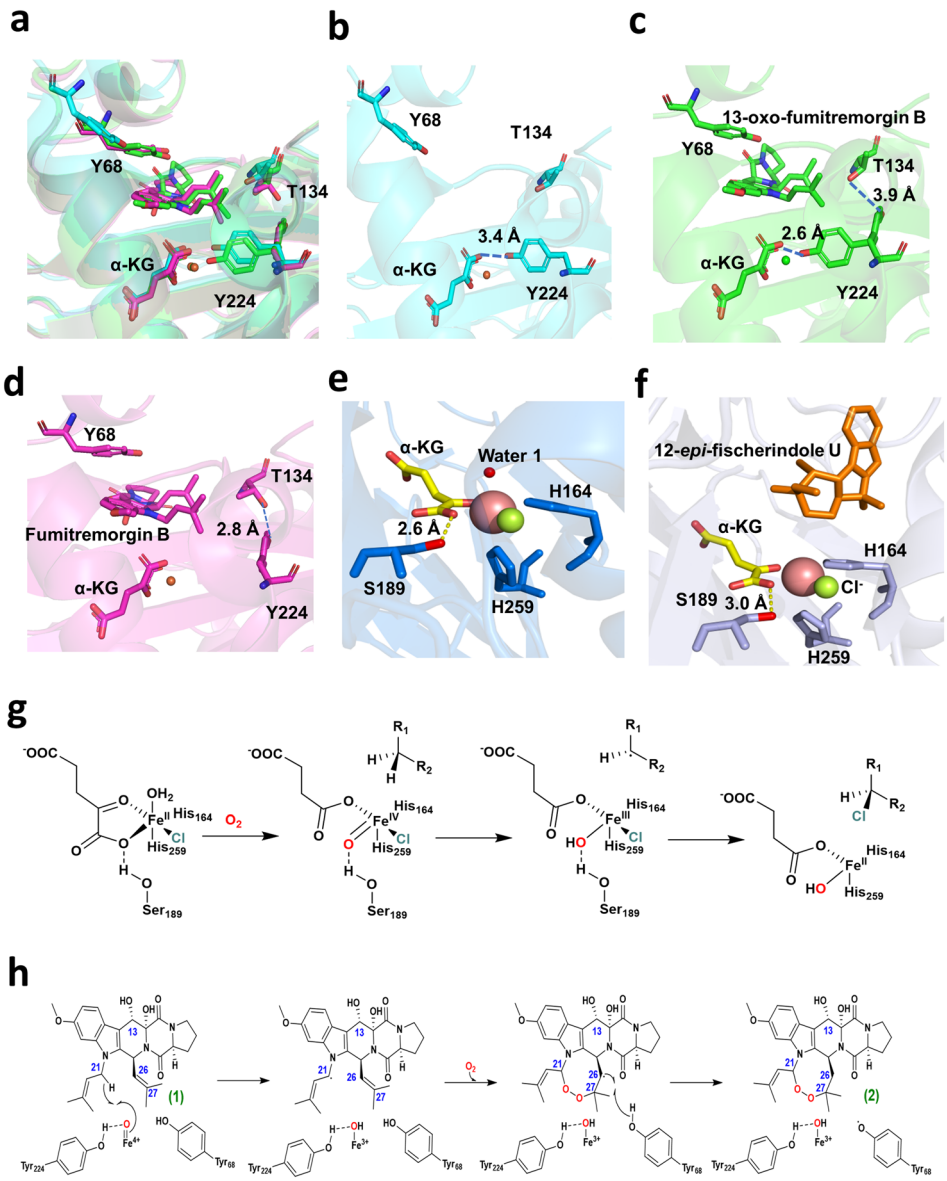

Fig. 2 Wild-type ftmOx1 displays endoperoxidation selectivity through Y224 forming H-bonds with α-KG and T134. (a–d) The substrate binding pocket in (a) the overlapped crystal structures of (b) the ftmOx1·Fe^{2+}·α-KG binary complex (pdb code 4Y5S, displayed in cyan), (c) ftmOx1·Co^{2+}·α-KG·13-oxo fumitremorgin B ternary complex (pdb code 7WSB, displayed in green) and (d) ftmOx1·Fe^{2+}·α-KG·fumitremorgin B ternary complex (pdb code 7ETK, displayed in pink). (e) Iron centre coordination mode in the crystal structure of WelO5 in complex with Fe^{2+} and α-KG (pdb code 5IQS). (f) Crystal structure of WelO5 in complex with Fe^{2+}, α-KG and the substrate 12-*epi*-fischerindole U (pdb code 5IQU). In (b–f), the distances are shown for the dotted lines indicating hydrogen-bond formation. In (b–d), Y224 of ftmOx1 has two conformations, one is fixed by forming a H-bond with T134 observed in (c) 7WSB and in (d) 7ETK, and the other conformation is fixed by forming a H-bond with α-KG observed in (b) 4Y5S and (c) 7WSB. (g) WelO5 displays chlorination selectivity by forming a H-bond with the oxy-ferry species. (h) FtmOx1 displays endoperoxidation by forming a H-bond with the oxy-ferry species. In (a–f), the structures of the proteins are displayed in 80% transparent cartoon mode. All residues are displayed in stick mode. The iron ion is represented as balls in orange (a, b, e and f) and in green (c). The Co^{2+} ion is orange in (d). The Cl^- ions are green in (e) and (f).

explain the mechanism of over-oxidized keto-product formation at the C-13 position, we also tried to co-crystalize the complex of the ftmOx1 Y224F variant with verruculogen (compound **2** in Scheme 1). However, finally, we only got the crystal structure of the apo ftmOx1 Y224F variant (pdb code 7DE0) (Fig. S3a, Table S1†). In this structure, four identical molecules of FtmOx1 Y224F are in each asymmetric unit (Fig. S3b†). The tetramer is composed of two kinds of dimers. One is a dimer with 'face-to-face contacts' at the C-terminus (Fig. S3c†), which is similar to those (Fig. S3d†) reported in the structures of ftmOx1·Fe^{2+} (4Y5T), the ftmOx1·Fe^{2+}·α-KG binary complex (4Y5S), the ftmOx1·Fe^{2+}·α-KG·fumitremorgin B ternary complex (7ETK), ftmOx1 Y140F·Fe^{2+} (6OXJ), and the ftmOx1 Y140F·Fe^{2+}·α-KG binary complex (6OXH).[2] The other is a dimer with 'point-to-point contacts' at the N-termini (Fig. S3e†), a new touch-folding observed for the ftmOx1 Y224F

variant. The structure of the ftmOx1 Y224F variant monomer is almost identical to its wild-type with an RMSD value of 0.30 Å (Fig. S3f†). The orientations of side-chains of residues Y224 and F224 are identical to each other (Fig. S3g and h†). On the whole, the crystal structure of apo ftmOx1 Y224F does not present us with useful information about how residue Y224 works in ftmOx1 catalytic reactions.

To address how residue Y224 works in the reactions, we had to excavate valuable information from the reported structures. Interestingly, in the structure of the ftmOx1·Fe^{2+}·α-KG binary complex (4Y5S), we found that the distance between the oxygen atom of Y224 –OH and one oxygen atom (ligated with Fe^{2+}) of one carboxyl group of α-KG was 3.4 Å (Fig. 2b). This indicates that residue Y224 most likely forms one weak hydrogen bond with the oxygen atom of the carboxyl group of α-KG. This H-bond was also observed in one conformation of Y224 in the structure of the ftmOx1·Co^{2+}·α-KG·13-oxo fumitremorgin B ternary complex (pdb code 7WSB, where the related distance is 2.6 Å in Fig. 2c),[4] and in the reported structures of the ftmOx1 Y68F ·Co^{2+}·α-KG binary complex (pdb code 7ETL, where the related distance is 3.0 Å in Fig. S4a†)[6] and the ftmOx1 Y140F·Fe^{2+}·α-KG binary complex (pdb code 6OXH, where the related distance is 3.5 Å in Fig. S4b†).[2] Due to the transient structures of reaction intermediate complexes ftmOx1·α-KG·Fe(IV)═O and ftmOx1·α-KG·Fe(III)–OH being unavailable, the hydrogen-bond between Y224 –OH and α-KG observed in the structures 4Y5S, 7WSB, 7ETL and 6OXH is thought to be evidence of a hydrogen bond formed between Y224 –OH and Fe(IV)═O or Fe(III)–OH active species, as suggested for the oxidase WelO5.[12]

WelO5 displays different selectivity of chlorination and hydroxylation on the substrate 12-*epi*-fischerindole U.[12] It was reported that wild-type WelO5 has chlorination selectivity, while its S189A variant displays hydroxylation selectivity.[12] The co-crystal structures of the binary complex WelO5·Fe^{2+}·α-KG (pdb code 5IQS) and of the ternary complex WelO5·Fe^{2+}·α-KG·12-*epi*-fischerindole U (pdb code 5IQU) (Fig. 2e and f)[12] demonstrate that the distances between the hydroxyl group of S189 and one oxygen atom (ligated with Fe^{2+}) of the carboxyl group of α-KG were 2.6 Å and 3.0 Å, respectively. Residue S189 forms one hydrogen bond with the oxygen atom of the carboxyl group of α-KG. When S189 was replaced by A189, the WelO5 S189A variant did not show any chlorination selectivity *vs.* hydroxylation. Therefore, S189 is a key factor in the conformational selectivity in the equatorial plane, bringing the precursor of the oxy-ferry intermediate to the equatorial conformation through hydrogen bonding (Fig. 2g). Similarly, for ftmOx1, in the absence of ascorbate, the potential hydrogen-bond between Y224 –OH and Fe(IV)═O or Fe(III)–OH species might block oxygen rebound reaction from Fe(III)–OH into the radical C21$^{\bullet}$, thus O_2 installation is preferred (Fig. 2h). When residue Y224 is replaced by F224,[13] the hydrogen-bond between Y224 and Fe(III)–OH is impaired or destroyed, thus Fe(IV)═O or Fe(III)–OH will be more active than in the case of the wild-type ftmOx1 catalyzed reaction, resulting in the oxygen rebound reaction being dominant (Scheme 1b). Therefore, Y224 acts as a critical element in the conformational selectivity in the equatorial plane, fixing the precursor of the oxy-ferry intermediate into the equatorial conformation.

Roles of residue T134 in ftmOx1 catalyzed reactions

As shown in Fig. 2d, in the structure of ftmOx1·Fe^{2+}·α-KG·fumitremorgin B (7ETK),[6] the side-chain –OH group of Y224 was found to be close to the residue T134 –OH with a distance of 2.8 Å. This observation implies that they form a hydrogen bond with each other. This hydrogen bond might also form in the structure of ftmOx1·Co^{2+}·α-KG·13-oxo fumitremorgin B (7WSB), although the distance mentioned above is 3.9 Å (Fig. 2c). As mentioned above, in structure 7WSB, Y224 has two conformations. One conformation of Y224 forms a hydrogen bond with α-KG, and the other might form a hydrogen bond with T134. As shown in Fig. 2a, the two conformers of Y224 in structure 7WSB overlapped well with the conformations of Y224 in structures 4Y5S and 7ETK, respectively. In contrast, in the structures of ftmOx1·Fe^{2+} (4Y5T) and the ftmOx1·Fe^{2+}·α-KG binary complex (4Y5S), the –OH groups of residues T134 and Y224 are all 6.4 Å far away (Fig. 3a). These findings reveal that T134 is involved in the catalytic reaction.

On one hand, as shown in Fig. S5,† when the structure of ftmOx1·Fe^{2+}·α-KG·fumitremorgin B (7ETK) was overlapped with the structure of ftmOx1·Fe^{2+}·α-KG (4Y5S), the distances between one methyl group at the C-21 allyl of fumitremorgin B in structure 7ETK and –OH group of Y224 in structure 4Y5S, and between this methyl group and one aromatic carbon of Y224 were only 2.1 Å and 2.2 Å, respectively. These short distances generate steric hindrance between the substrate and residue Y224 after the substrate completely inserts into the iron ion binding pocket, leading to rotation of Y224. Structure 7WSB indicates that substrate insertion into the iron-binding pocket results in rotation of partial Y224 to the position where it can form a hydrogen bond with T134. Therefore, during ftmOx1 catalysis, the conformation of Y224 is firstly fixed by forming a weak hydrogen-bond with α-KG and then by forming a hydrogen bond with residue T134. In other words, the hydrogen bond between Y224 and T134 might stimulate Y224 rotation, while the hydrogen bond between Y224 and α-KG might block Y224 rotation. The steric effects from the insertion of the substrate fumitremorgin B into the iron ion binding center force residue Y224 to rotate. The balance among these three factors results in the rotation of Y224 in ftmOx1 catalyzed reaction. The endoperoxidation reaction happens at the beginning of the substrate insertion into the ion binding center.

On the other hand, as shown in Fig. 2a, when the structures of the binary complex ftmOx1·Fe^{2+}·α-KG (4Y5S), and of the ternary complexes ftmOx1·Fe^{2+}·α-KG·fumitremorgin B (7ETK) and ftmOx1·Co^{2+}·α-KG·13-oxo fumitremorgin B (7WSB) are superimposed, the positions of

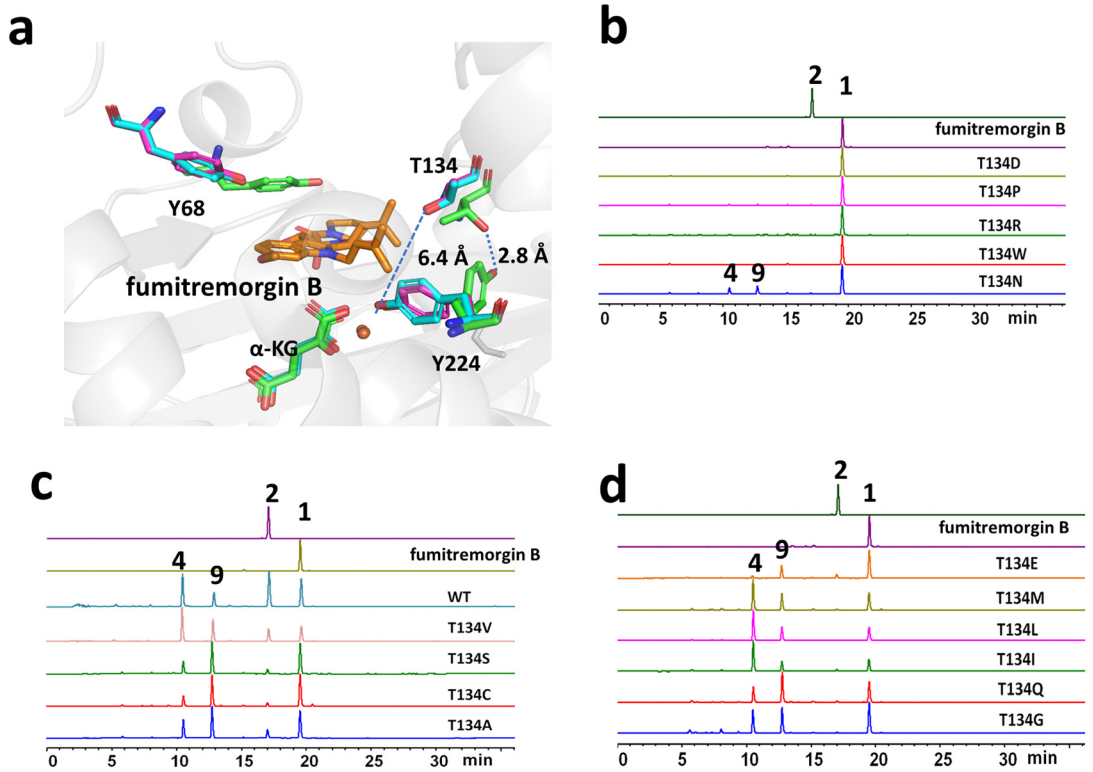

Fig. 3 Residue T134 acts as a regulator of the catalytic reaction. (a) T134 forms a H-bond with Y224 (in green stick) in structure 7ETK, but not in the structures of ftmOx1·Fe^{2+} (4Y5T in pink stick) and the ftmOx1·Fe^{2+}·α-KG binary complex (4Y5S in cyan stick). The conformational changes were detected upon overlapping these three structures (in grey and 80% transparent cartoon mode). Residues Y68, T134 and Y224, α-KG and the substrate (orange) are displayed in stick mode. The balls represent iron ions. (b–d) The enzymatic reactions of the wild-type ftmOx1 and its single-site directed variants of T134, detected using a HPLC system.

residue T134 are almost the same. However, the orientations of the methyl group and –OH group of T134 are different in structures 7ETK and 7WSB. This might be due to the low resolution (2.87 Å) of the reported structure 7WSB.[4] The orientations of the methyl group and –OH group of T134 in 7WSB are the same as those of T134 in structure 4Y5S (Fig. 2b and c), but different from those of T134 in structure 7ETK (Fig. 2c and d and S6†). As shown in Fig. S6,† in structures 7ETK and 7WSB, the distances from the methyl group of T134 to the methyl groups at C-24 were measured to be 4.4 Å and 5.4 Å, to the methyl groups at C-25 were measured to be 3.9 Å and 4.9 Å, to the methyl groups at C-28 were measured to be 4.1 Å and 5.7 Å, and to the methyl groups at C-29 were measured to be 4.1 Å and 4.9 Å of fumitremorgin B and its analogue 13-oxo fumitremorgin B, respectively. The methyl groups at the C-24, C-25, C-28 and C-29 positions of 13-oxo fumitremorgin B are very hydrophobic, so it seems inacceptable that the hydrophilic –OH group of T134 in 7WSB should point to these methyl groups of 13-oxo fumitremorgin B. Therefore, if we exclude the potential errors in the orientations of T134 side-chains in structure 7WSB, T134 should undergo hydrophobic interactions with the substrate or its analogue, which is also very important for ftmOx1 catalyzed reactions.

To confirm the roles of residue T134 in the ftmOx1 catalytic reaction, we then performed its site-directed mutagenesis studies. As summarized in Scheme 1g and h and displayed in Fig. 3b–d, under the condition of excess Fe^{2+}, O_2, α-KG and ascorbate, the main products of the ftmOx1 catalyzed reaction are compounds **2** and **4**. Their chemical structures were ascertained using 1D ^{1}H-NMR spectra and comparison of the chemical shifts of the ^{1}H and ^{13}C atoms with those previously reported.[2,4] Compound **4** is produced from the oxygen rebound and deprenylation reaction.[2] When residue T134 was switched to residue G134, the main products were compounds **4** and **9** (Fig. 3d). The chemical structure of compound **9** was characterized using mass spectrum and NMR techniques (Fig. S7 and Table S2†). When T134 was mutated into hydrophilic residue Asp, Arg and Asn, or steric residues Pro and Trp, the repulsive interactions between T134 and the substrate or its analogue led to the substrate or its analogue not being able to insert into the iron ion binding pocket, and thus almost no catalytic reactions happened. When T134 was replaced by Val, Met, Leu and Ile, the hydrogen bond between T134 and Y224 was completely destroyed, but the hydrophobic interaction with the substrate or its analogue was enhanced, and the main product became compound **4**. When residue T134 was substituted by residues Ser, Cys, Ala and Gln, both

hydrophobic interaction and hydrogen bond interaction became weaker, and the main product was compound **9**. In a word, the mutations from T134 into other residues destroy or weaken the hydrogen bond between Y224 and T134, and Y224 becomes more flexible than in the wild-type ftmOx1. At the same time, the hydrophobic or steric interactions between the substrate and T134 will also be changed depending on the nature of the mutated residue. These effects will decrease the possibility of Y224 forming a hydrogen bond with the Fe(IV)=O species during substrate insertion into the iron ion binding pocket. Therefore, the number of Fe(III)–OH active species will be increased and the oxygen rebound reaction and dealkylation will be enhanced (Scheme 2).

Identically, when Y224 was mutated into Phe, the Fe(IV)=O species could not be stabilized by Y224 in the beginning of the catalytic reaction. The number of Fe(IV)=O or Fe(III)–OH species was thus increased, which resulted in the oxygen rebound reaction occurring easily at the beginning of the substrate insertion into the iron binding centre. When the substrate completely inserts into the iron binding pocket, the hydrogen-bond interaction between Y224 and T134 is also destroyed. Then, the conformation of the side-chain of F224 will become extremely flexible. Moreover, the size of the side-chain of F224 is smaller than that of Y224, thus the substrate insertion into the iron ion binding pocket will be easier in the ftmOx1 Y224F variant than in wild-type ftmOx1. The Fe(IV)=O species will have more chances to perform HAT from C-21 of the substrate (Scheme 2). The main product switches to oxygen rebound reaction products 4 and 9. Therefore, T134 acts as a regulator in ftmOx1 catalysed reactions, mediating the direction of the reaction by hydrogen-bonding with Y224 and by hydrophobic interactions with the substrate. Y224 further determines the selectivity of the catalytic reaction by stabilizing the conformation of Fe(IV)=O or Fe(III)–OH species. In the whole ftmOx1 catalysed reaction, the chances for Y224 to form the radical Y224-O$^{\bullet}$ are blocked by forming hydrogen bonds with the Fe(IV)=O species and with the T134 –OH group.

Roles of residue Y68 in ftmOx1 catalyzed reactions

As shown in Fig. 2a, compared to the conformation of Y68 in the structure of ftmOx1·Fe^{2+}·α-KG (4Y5S), Y68 shifts to the top of the substrate (in the structure of ftmOx1·Fe^{2+}·α-KG·fumitremorgin B, 7ETK) or its analogue (in the structure of ftmOx1·Co^{2+}·α-KG·13-oxo fumitremorgin B, 7WSB) through hydrophobic interactions between the Y68 side-chain and rings B and C of the substrate or its analogue. As shown in Fig. S5,† in structures 4Y5S and 7ETK, the distances between

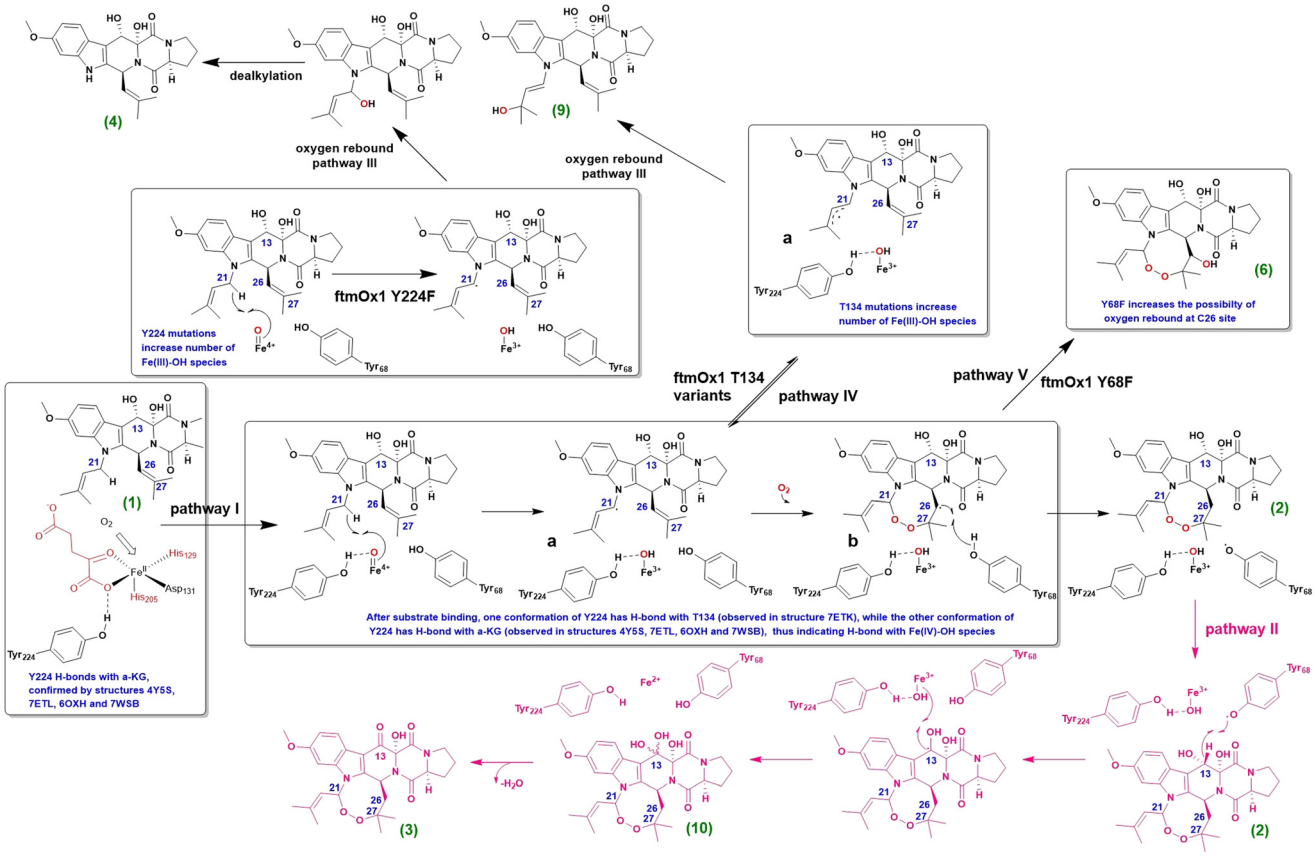

Scheme 2 Proposed mechanisms for ftmOx1 and its variant involved reactions under different conditions. Pathway II cannot explain how compound **2** is directly oxidized into 3 by ftmOx1 (Scheme 1g), therefore it is shown in red.

the oxygen atom of the Y68 –OH group and C-13, C-21 or C-26 atom of the substrate were observed to change from 4.0 Å to 3.7 Å, from 7.2 Å to 6.3 Å, and from 6.5 Å to 4.0 Å, respectively. These distance changes result from the location of residue Y68 on a very flexible region. The shorter distances (3.7 Å and 4.0 Å) indicate that, in the substrate and α-KG's specific binding status, Y68 is very conducive to donation of hydrogen to the radical C-26• (pathway I in Scheme 2) and oxidation of the hydroxy group at C-13 group (*i.e.*, Y68-O• performs hydrogen-abstraction from the C-13 atom) (pathway II in Scheme 2).

In pathway I, residue Y68 provides a hydrogen atom to the C26• radical (generating Y68-O•), and the major product verruculogen is produced. In pathway II, radical Y68-O• abstracts hydrogen from the C-13 atom, followed by hydroxyl group rebound reaction from Fe(III)–OH species into the radical C-13•, forming an unstable geminal diol containing intermediate. Although it is hard to separate this intermediate from the reaction system, we still detected a compound **10** with a molecular formula $C_{27}H_{33}N_3O_8$ and a molecular weight 528 by ESI-HR-MS assay (Fig. S8†). Its molecular weight is consistent with the geminal diol containing product, confirming oxidation of the hydroxyl group at the C-13 position. This geminal diol intermediate will be easily dehydrated to form over-oxidized keto-product compound **3**.

In contrast, in structure 7ETK, the distance between the oxygen of the Y224 hydroxyl group and O-2 atom of the carboxyl group of α-KG is 8.7 Å. Moreover, the distances between the oxygen atom of the Y224 –OH group and C-13, C-21 or C-26 were measured to be 12.4 Å, 8.3 Å and 8.9 Å, respectively. Due to these unfavorable distances, Y224 observed in structure 7ETK cannot participate in ftmOx1 catalytic reaction after the substrate completely inserts into the iron ion binding pocket. In structure 7WSB, Y224 displays two conformations, one is almost the same as that observed in 7ETK, although the distance (3.9 Å) between Y224 –OH and T134 –OH is a little larger than that (2.8 Å) in structure 7ETK (Fig. 2c and d). The other is close to a metal ion center, but it forms H-bonds with α-KG, and its position is almost identical to that in structure 4Y5S (Fig. 2a). Therefore, the –OH group of Y224 is obviously locked by forming H-bonds with α-KG and residue T134, which makes it impossible for Y224 to participate in ftmOx1 catalytic reactions. Thus, only Y68 acts as a hydrogen donor of C26• and is able to perform oxidation of the –OH group at the C-13 position.

Possible pathways of ftmOx1 catalyzed reactions

To uncover the mechanism of ftmOx1 involved reactions, we list several possible pathways in Scheme 2. Since the first tyrosine radical has already been proven to be formed at residue Y68 during O_2 installation,[2] pathway I was suggested, in which the hydroxyl group of Y224 stabilizes Fe(III)–OH species by forming hydrogen bonds during catalytic reaction, as observed in the structures of ftmOx1·Fe^{2+}·α-KG (4Y5S), the ftmOx1·Co^{2+}·α-KG·13-oxo fumitremorgin B ternary complex (7WSB), ftmOx1 Y68F ·Co^{2+}·α-KG (7ETL) and ftmOx1 Y140F·Fe^{2+}·α-KG (6OXH). This specific function is similar to the role of residue S189 of WelO5 in chlorination selectivity.[12] The highly active oxyferry species abstracts hydrogen from the C-21 atom of the substrate fumitremorgin B. The hydroxyl group of Y224 further stabilizes the Fe(III)–OH species. This step suppresses oxygen rebound reaction and promotes dioxygen addition to a large extent. Once dioxygen installation happens, the radical C21• is transferred to the C-26 atom (forming C26•). Residue Y68 then provides a hydrogen atom to the C26• radical, and the major product verruculogen is produced in the presence of the reductant. After that, if there is not enough reductant (for example, ascorbic acid) to quench this radical, as shown in pathway II, the Y68 radical (Y68-O•) would abstract hydrogen from C-13 followed by hydroxyl group rebound reaction from Fe(III)–OH species into the radical C13•, forming an unstable geminal diol containing intermediate (compound **10**). This geminal diol intermediate will be easily dehydrated to form over-oxidized keto-product compound **3**.

When Y224 is replaced by F224, the hydrogen bond between Y224 and α-KG will be destroyed, then the number of Fe(IV)═O species will be increased, which conduct HAT from the C-21 position of the substrate (forming the radical C21•), followed by oxygen rebound and dealkylation (pathway III). When T134 is mutated into other residues, the hydrogen bond between Y224 and T134 becomes weak or abolished. The rotation of Y224 will become more difficult than in wild-type ftmOx1, and the number of Y224 non-stabilized Fe(III)–OH species increases, which will enhance oxygen rebound reaction (pathway IV). In either the presence or absence of ascorbate, the main product of the ftmOx1 Y68F catalytic reaction is compound **6** (Scheme 1d),[2,5] which follows pathway V. In pathway V, after O_2 insertion, the C26• radical forms; because residue F68 cannot donate hydrogen, the oxygen rebound reaction will then happen, which produces compound **6**. Pathway II demonstrates that, in the absence of ascorbate, consumption of the substrate is almost equal to that of the enzyme during the catalytic reaction. This accords well with the equivalent molar ratio of ftmOx1 and the substrate used in the catalytic reactions in Scheme 1. It also conforms to the fact that the major product of the catalytic reaction is compound **3** in the absence of reductant.

However, it was reported that compound **2** could be directly oxidized into compound **3** in the absence of ascorbate, and into compound **8** in the presence of ascorbate (Scheme 1f).[4] But in structures 7ETK and 7WSB (Fig. S6†), the distance between Fe^{2+} and the C-13 atom of the substrate was measured to be 8.1 Å and 7.4 Å, both of which are unfavorable for Fe(IV)═O species to perform HAT directly from the C-13 atom, generating C-13• as suggested in pathway II. Similarily, ftmOx1 can perform direct oxidation of 13-oxo

fumitremorgin B (compound 7) into compound **5** in Scheme 1e,[4] which does not produce compound **3**, when Y224 forms hydrogen bonds with α-KG and T134. The reactions in Scheme 1e and f appear to be solid evidence of a COX-like mechanism for the ftmOx1 catalyzed reaction. In addition, in the presence of ascorbate, the main product of ftmOx1 Y224F catalyzed reaction on compound **1** is compound **2**, which cannot be validated by the mechanism shown in Scheme 2. Therefore, to uncover the mechanism of the ftmOx1 involved reactions, extra experiments should be performed in the future such as co-crystalization of the ftmOx1·Fe^{2+}·α-KG·verruculogen ternary complex in the absence of O_2 or the ftmOx1·Co^{2+}·α-KG·verruculogen ternary complex in the presence of O_2, or more kinetic experiments or molecular simulation than those reported previously.[2,5,6,14]

Conclusions

Taken together, in this study, we conducted structure-based analysis on the mechanism of the complicated ftmOx1 catalytic reactions. Firstly, analysis of the reported structures of the three binary complexes ftmOx1·Fe^{2+}·α-KG (4Y5S), ftmOx1 Y68F·Co^{2+}·α-KG (7ETL) and ftmOx1 Y140F·Fe^{2+}·α-KG (6OXH), and of the two ternary complexes ftmOx1·Fe^{2+}·α-KG·fumitremorgin B (7ETK) and ftmOx1·Co^{2+}·α-KG·13-oxo fumitremorgin B (7WSB) suggested that a hydrogen bond formed between the Y224 –OH group and one carboxyl group of α-kG. This carboxyl group of α-kG ligates with Fe^{2+} before and after the Fe(IV)═O species is formed. Y224 enhances the selectivity of ftmOx1-involved catalytic endoperoxidation reaction by stabilizing the conformation oxy-ferry species through hydrogen bonding. This step potentially suppresses oxygen rebound reaction, and explains why the replacement of residue Y224 by F224 results in the formation of major products compounds **4** and **5** in the absence of ascorbate. Secondly,^{19}F-NMR experiments revealed that a new conformation of residue Y224 is generated due to substrate insertion into the Fe^{2+} binding centre. This result is consistent with the structures of ftmOx1·Fe^{2+}·α-KG·fumitremorgin B (7ETK) and ftmOx1·Co^{2+}·α-KG·13-oxo fumitremorgin B (7WSB). In structure 7ETK, a hydrogen bond between T134 and Y224 was observed, which stabilizes the conformation of Y224, further preventing it from forming the Y224-O$^{\bullet}$ radical during ftmOx1 catalytic reaction. Residue T134 also forms hydrophobic interactions with the substrate. It acts as a key determinant of ftmOx1 catalysed endoperoxidation. Therefore, in the whole mechanism (Scheme 2), the oxy-ferry species directly abstracts a hydrogen proton from the C-21 atom, and Y68 works as a hydrogen donor, generating compound **2**. Then, compound **2** is probably further oxidized by the radical Y68$^{\bullet}$ into compound **3**, which supports a CarC-like catalytic mechanism. However, this mechanism cannot account for how compounds **2** and **7** are directly oxidized into compound **3** or **8**, and **5** by ftmOx1, respectively. Either of these reactions could be thought as evidence of the COX-like mechanism. In a word, different from either the COX-like mechanism or CarC-like mechanism, the current study displays the roles of residues Y68, T134 and Y224 in the catalytic reaction. Based on this, it is possible to design non-haem iron enzymes for product diversity.

Experimental section

Materials and methods are described in detail in the ESI,† which is available on the website of the journal.

Author contributions

F. W. did most studies of ftmOx1. Y. G. and J. G. solved the X-ray structure of the ftmOx1 variant. W. L. helped perform ^{19}F-NMR spectroscopy. C. C. designed the whole project and wrote the manuscript.

Conflicts of interest

There are no conflicts to declare.

Acknowledgements

This work was supported by National Program on Key Basic Research Project of China with number 2017YFE0108200, the National Science Foundation of China (NSFC) (21977110, 22174155 and 22177127) and SIOC self-deployment project under No. sioczz202204. The authors thank the facility team members of Shanghai Synchrotron Radiation Facility (SSRF), China, for X-ray crystal data collection, and NMR facility team of Wuhan Institute of Physics and Mathematics, Chinese Academy of Sciences (CAS), for NMR data collection.

References

1 M. Bu, B. B. Yang and L. Hu, *Curr. Med. Chem.*, 2016, **23**(4), 383–405.
2 N. P. Dunham, J. M. Del Rio Pantoja, B. Zhang, L. J. Rajakovich, B. D. Allen, C. Krebs, A. K. Boal and J. M. Bollinger, Jr., *J. Am. Chem. Soc.*, 2019, **141**(25), 9964–9979.
3 N. Steffan, A. Grundmann, S. Afiyatullov, H. Ruan and S. M. Li, *Org. Biomol. Chem.*, 2009, **7**(19), 4082–4087.
4 G. Zhu, W. Yan, X. Wang, R. Cheng, N. Naowarojna, K. Wang, J. Wang, H. Song, Y. Wang, H. Liu, X. Xia, C. E. Costello, X. Liu, L. Zhang and P. Liu, *JACS Au*, 2022, **2**(7), 1686–1698.
5 C.-L. Lin, A. L. M. Hernandez, T. N. Laremore, A. Silakov, C. Krebs, A. K. Boal and J. M. Bollinger, *ACS Catal.*, 2022, **12**(12), 6968–6979.
6 L. Wu, Z. Wang, Y. Cen, B. Wang and J. Zhou, *Angew. Chem., Int. Ed.*, 2022, e202112063.
7 C. A. Rouzer and L. J. Marnett, *J. Lipid Res.*, 2009, **50**(Suppl), S29–S34.
8 J. N. Ji and S. L. Chen, *Phys. Chem. Chem. Phys.*, 2018, **20**(41), 26500–26505.

9 M. A. Lima, R. P. Cavalheiro, G. M. Viana, M. C. Z. Meneghetti, T. R. Rudd, M. A. Skidmore, A. K. Powell and E. A. Yates, *Glycoconjugate J.*, 2017, **34**(3), 405–410.
10 J. L. Kitevski-LeBlanc and R. S. Prosser, *Prog. Nucl. Magn. Reson. Spectrosc.*, 2012, **62**, 1–33.
11 L. Yu, P. J. Hajduk, J. Mack and E. T. Olejniczak, *J. Biomol. NMR*, 2006, **34**(4), 221–227.
12 A. J. Mitchell, Q. Zhu, A. O. Maggiolo, N. R. Ananth, M. L. Hillwig, X. Liu and A. K. Boal, *Nat. Chem. Biol.*, 2016, **12**(8), 636–640.
13 X. Wang, H. Su and Y. Liu, *Phys. Chem. Chem. Phys.*, 2017, **19**(11), 7668–7677.
14 A. Milaczewska and T. Borowski, *Dalton Trans.*, 2019, **48**(43), 16211–16221.